

# Exciton interaction induced spin splitting in MoS<sub>2</sub> monolayer

Yao Li,<sup>1</sup> G. Li,<sup>2,3,\*</sup> Xiaokun Zhai,<sup>4</sup> Shi Fu Xiong,<sup>4</sup> Hongjun Liu,<sup>4</sup> Xiao Wang,<sup>5</sup> Haitao Chen,<sup>6</sup> Ying Gao,<sup>1</sup> Xiu Zhang,<sup>1</sup> Tong Liu,<sup>7</sup> Yuan Ren,<sup>7</sup> Xuekai Ma,<sup>8</sup> Hongbin Fu,<sup>1</sup> and T. Gao<sup>1,†</sup>

<sup>1</sup>Tianjin Key Laboratory of Molecular Optoelectronic Science, Institute of Molecular Plus, School of Science, Tianjin University, Tianjin 300072, China

<sup>2</sup>School of Physics and Astronomy, Monash University, Victoria 3800, Australia

<sup>3</sup>ARC Centre of Excellence in Future Low-Energy Electronics Technologies, Monash University, Victoria 3800, Australia

<sup>4</sup>Institute of Functional Crystals, Tianjin University of Technology, Tianjin 300384, China

<sup>5</sup>Key Laboratory for Micro-Nano Physics and Technology of Hunan Province,

School of Physics and Electronics, Hunan University, Changsha, Hunan, 410012, China

<sup>6</sup>College of Advanced Interdisciplinary Studies, National University of Defence Technology, Changsha, 410073, Hunan, China

<sup>7</sup>Department of Aerospace Science and Technology,

Space Engineering University, Beijing 101416, China

<sup>8</sup>Department of Physics and Center for Optoelectronics and Photonics Paderborn (CeOPP), Universität Paderborn, Warburger Strasse 100, 33098 Paderborn, Germany

By pumping nonresonantly a MoS<sub>2</sub> monolayer at 13 K under a circularly polarized cw laser, we observe exciton energy redshifts that break the degeneracy between B excitons with opposite spin. The energy splitting increases monotonically with the laser power reaching as much as 18 meV, while it diminishes with the temperature. The phenomenon can be explained theoretically by considering simultaneously the bandgap renormalization which gives rise to the redshift and exciton-exciton Coulomb exchange interaction which is responsible for the spin-dependent splitting. Our results offer a simple scheme to control the valley degree of freedom in MoS<sub>2</sub> monolayer and provide an accessible method in investigating many-body exciton exciton interaction in such materials.

Transition metal dichalcogenides (TMDs) attracted great attention recently because of their unique photonic and optoelectronic properties [1–3]. When a bulk TMD is thinned down to a monolayer (ML), it becomes a direct bandgap material with gaps located at  $K$  and  $K'$  points [4, 5] in the corners of the Brillouin zone. Owing to the spin-orbit interactions, each valley is spin-split, resulting in two distinct exciton resonances denoted as A and B excitons [5, 6]. TMD excitons' binding energy (about 0.5 eV) is much larger than that of GaAs (10 meV), with a smaller Bohr radius  $a_B$  (1 nm *vs.* 10 nm), so that their excitonic features are robust even at room temperature [3], and providing a solid platform to investigate exciton physics over a broad range of temperature and excitation density [7–9]. Since the states in the  $K$  and  $K'$  valley are related with each other by time-reversal symmetry, the corresponding exciton energies of the same type from different valley are degenerate [4, 10, 11]. In the interest of engineering TMD based valleytronic devices, it is desirable to lift the energy degeneracy to make use of the valley degree of freedom [12]. In experiments, it has been demonstrated that the exciton degeneracy can be broken by an out-of-plane magnetic field up to 10 T [13–19]. Such apparatus, however, might not be applicable in the realistic applications.

Another experimentally accessible method to lift the degeneracy is employing the optical Stark effect [20, 21].

When a pulsed laser pump the TMD ML with energy just below the exciton resonance, the hybridization between the equilibrium state and the photon-dressed state will shift the exciton to a larger energy. By applying a pulsed probe laser to measure the change of absorption/reflection spectra, the exciton energy degeneracy between different valleys is lifted if the pump laser is circularly polarized [20, 21], which is supposedly equivalent to a 60 T pseudomagnetic field for a 10 meV splitting. This approach, however, not only requires high laser power (GW/cm<sup>2</sup>) but also it is intrinsically transient, which can only reveal a TMD ML's dynamical properties within the pump pulse duration. Therefore, an optically-tunable exciton splitting scheme applicable to the equilibrium scenario in the TMD ML is still missing.

In this work, we demonstrate experimentally that the energy degeneracy of excitons of the same type of different valley in a MoS<sub>2</sub> ML can be broken by the spin-dependent exciton-exciton interactions via a circularly polarized cw pump at 13 K. The laser energy is 230 meV larger than the exciton resonance in MoS<sub>2</sub> ML. The spin splitting can be tuned from 0 to 18 meV under the pump power of 0.3 MW/cm<sup>2</sup>. Theoretically, the splitting results from the disagreement of exciton-exciton interaction between different valley which raises the exciton energies differently [22], on top of an overall band gap renormalization given by free carries [23, 24]. Our results offer a new way to control the valley degree of freedom, and could be directly applicable to TMD ML exciton-polariton systems [25, 26].

*Experiment.* A piece of MoS<sub>2</sub> ML is grown at 760 K by the chemical vapor deposition (CVD) on a SiO<sub>2</sub>/Si sub-

\*guangyao.li@monash.edu

†tinggegao@tju.edu.cn

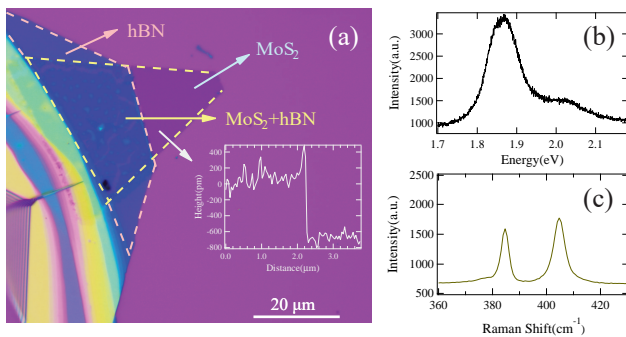


FIG. 1: Optical characterization of the sample. (a) AFM mapping of the MoS<sub>2</sub> ML, where the inset shows the thickness of the sample is about 0.7 nm. (b) PL spectrum of the MoS<sub>2</sub> ML excited by a 532 nm laser at room temperature. (c) Raman spectrum of the sample at room temperature.

strate. To protect the ML, a hBN layer with thickness of around 10 nm is transferred on top of the sample, shown in the atomic force microscopy (AFM) characterization in Fig. 1(a). We measure the optical spectrum of the MoS<sub>2</sub> ML by a home-built confocal PL setup (see Supplemental Material for more details) and obtain smooth PL spectra originated from the recombination of A excitons (1.865 eV) and B excitons (2.024 eV), as demonstrated in Fig. 1(b). The energy difference between A and B excitons of about 0.159 eV agrees with previous measurements [27–30]. Fig. 1(c) shows the Raman spectrum measured at room temperature by a commercial Raman microscope (WITec alpha 300), and the peak at 384.67 cm<sup>-1</sup> confirms the good quality of the MoS<sub>2</sub> ML.

To study exciton-exciton interactions, the sample is cooled down to 13 K by a cryogen free cryostat (Janis). We use a 532 nm laser (Spectra Physics) as the excitation source. The laser can be adjusted from linear to circular (left-handed or right-handed) polarization by using a quarter waveplate. The laser is focused on the sample through an objective with a spot of around 2 μm, and the emitted photons are collected by the same objective. A quarter waveplate, half waveplate and a linear polarizer are combined to resolve the polarization of the emitted PL from the sample. The polarization of photons is calculated by  $P = (I^+ - I^-)/(I^+ + I^-)$ , where  $I^+$  and  $I^-$  denote the counts of the right-hand and left-handed circularly polarization components.

At 13 K, the energies of A and B excitons are blueshifted to 1.948 eV and 2.099 eV respectively, and the trion peak appears at 1.911 eV [31] under the pump density of 0.008 MW/cm<sup>2</sup>, see Fig. 2(a). During the experiment, a mechanical chopper with a duty cycle of 5% is used to reduce possible heating effect by the laser. When the pump power is continuously increased, the spectrum peaks corresponding to exciton energies shift to lower values, i.e. redshifted, see Fig. 2(b). Similar redshift of the exciton energy has been reported previ-

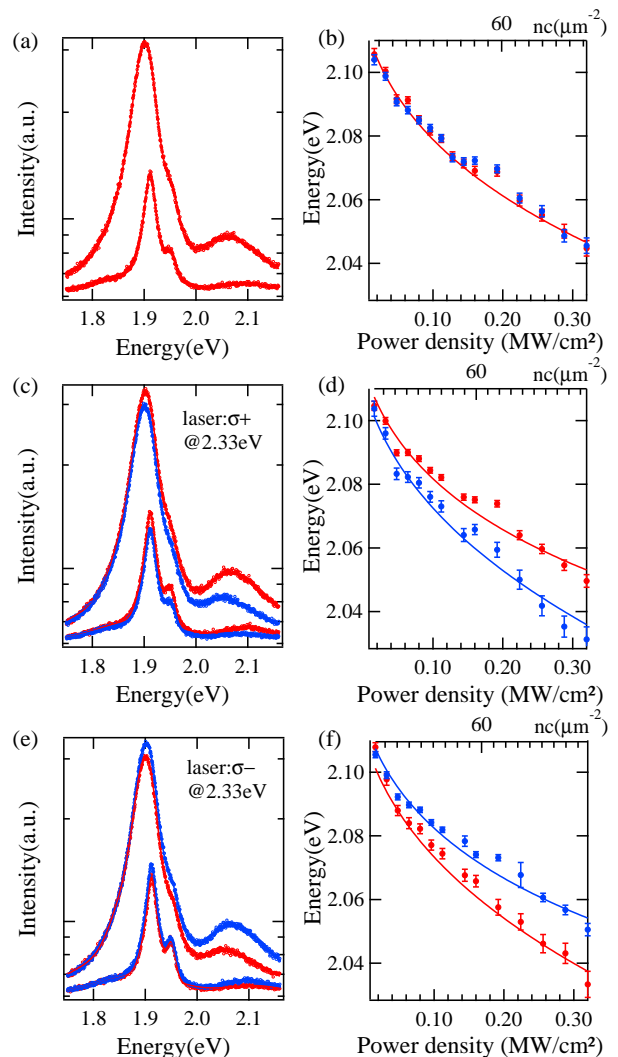


FIG. 2: The spectrum of the MoS<sub>2</sub> monolayer as a function of the pumping power. (a)(c)(e) Optical spectrum of the sample pumping by a linearly polarized, right-handed circularly polarized, and left-handed circularly polarized laser respectively, with density of 0.03 MW/cm<sup>2</sup> and 0.3 MW/cm<sup>2</sup>. (b)(d)(f) PL peaks (fitted B exciton energy) against the pumping power density (bottom axis), with polarization matching the corresponding spectra on the left columns. Red (blue) dots correspond to B (B') excitons. Solid curves are the theoretical plots against  $n_c$  (top axis) according to Eq. (3). Theory parameters can be found in [32].

ously in [9], where the anomalous blueshift and redshift crossover was measured by a pump-probe spectroscopy with a WS<sub>2</sub> ML and it was interpreted phenomenological by a Lennard-Jones potential between excitons [9]. In our current experiment, we did not observe the redshift-blueshift crossover.

Next we discuss the exciton energy changes with the spin degree of freedom. Since the A exciton peak overlaps with the trion peak [31] and it was demonstrated that the valley polarization effect of B excitons is stronger than

that of A excitons [30], here we focus on B excitons for the spin-split effect and sometimes refer them simply as excitons. Figure 2(c) shows the PL spectra of the MoS<sub>2</sub> ML pumping by a right-hand circularly polarized laser. The non-zero left-hand polarized PL is presumably caused by intervalley scattering [21], and the polarization  $P$  of B excitons is about 30% in agreement with [30]. By examining the spectral peak positions of each polarization component, we find an energy splitting about 18 meV under the pump power of 0.3MW/cm<sup>2</sup>. The energy splitting is reversed when the pump switches to the opposite polarization, see Fig. 2(e). In both cases, the energy of the co-polarized component is always higher than that of the cross-polarized component, in contrast to the results of MoSe<sub>2</sub>/WSe<sub>2</sub> heterostructures [33]. When the pump laser is linearly polarized, the energy splitting between two circularly polarized components disappears, see Fig. 2(a)(b).

The spin dependent energy splitting can be explained by the exciton-exciton interaction originated from the Coulomb interaction between electrons and holes. Simply speaking, the population imbalance between B excitons in different valley gives rise to a different energy correction because of the Coulomb interaction. Similar splitting can also be found in conventional semiconductor quantum well systems such as GaAs or InAs [22, 34–37]. However, the spin splitting observed is created under pulsed excitation and greatly reduced when the laser is tuned far away from the exciton resonance [35]. Thanks to the spin valley locking mechanism, the laser energy to induce the exciton splitting can be much larger (230meV) than the exciton resonance in MoS<sub>2</sub> ML, this leaves greater flexibility for the laser choice to control the valley degrees of freedom.

Compared with the optical Stark effect [20, 21] in the TMDs ML, the exciton splitting can be manipulated under much lower CW pumping density. In supplemental materials, we plot the exciton splitting as a function of the pumping density. The exciton splitting reaches 18 meV at the pumping density of around 0.3MW/cm<sup>2</sup>, around four orders of magnitude smaller than the optical Stark effect [21]. In addition, we can tune the exciton splitting from zero to 18meV continuously, which cannot be realized in [33]. Thus, the interexcitonic exchange interaction offers to tune the exciton splitting more effectively and stably in MoS<sub>2</sub> ML. In the following we develop a theory to model the energy splitting of the MoS<sub>2</sub> ML under various pumping configurations.

*Theory.* The measured exciton PL peak energy  $E_{PL}$  corresponds to recombination of electrons in the conduction band with the bound holes in valence bands, which can be written as  $E_{PL} = E_g + (-E_B)$ , where  $E_g$  is the bandgap and  $-E_B$  is the exciton binding energy. With increased carrier density, it has been shown that the excessive free carriers will result in bandgap renormalization and screening of  $-E_B$  [9]. First we look at

the bandgap renormalization. After taking the random phase approximation and quasi-static approximation, the energy reduction of the bandgap can be expressed as [23, 24]:

$$\Delta E_g(n_c) = V_s(k_F) n_c + \sum_{\mathbf{q}} [V_s(\mathbf{q}) - V(\mathbf{q})], \quad (1)$$

where  $n_c$  is the free carrier density (assuming  $n_e = n_h = n_c$ ),  $k_F = (2\pi n_c)^{1/2}$  is the 2D Fermi wave number,  $V(\mathbf{q}) = e^2/(2\epsilon_0 q)$  is the unscreened 2D Coulomb potential in SI unit with  $\epsilon_0$  the background permittivity, and  $V_s(\mathbf{q}, \omega) = V(\mathbf{q})/\epsilon(q, \omega)$  is the screened Coulomb potential. The screening effect can be simplified by the plasmon-pole approximation:  $1/\epsilon = 1 + \omega_{pl}^2/[(\omega + i\delta)^2 - \omega_q^2]$ , where  $\omega_{pl}(q) = [2\pi e^2 n_c q / (\epsilon_0 m_r)]^{1/2}$  is the plasma frequency with  $m_r$  the reduced electron-hole mass,  $\omega$  is the light frequency,  $\delta$  is a small number that shifts the pole away from the real axis,  $\omega_q^2 = \omega_{pl}^2(1 + q/\kappa) + \nu_q^2$ , and  $\nu_q^2 = C[\hbar q^2 / (4m_r)]^2$ ;  $\kappa = \frac{2\pi e^2}{\epsilon_0} \sum_{e,h} \frac{\partial n_{e,h}}{\partial \mu_{e,h}}$  is the screening wave number, with  $\mu_{e,h}$  and  $n_c$  related by the Fermi function [24].

Next we look at screening and spin imbalance effects on the exciton energy. The exciton binding energy will reduce to  $-E_B/\epsilon_r^2$  because of screening [38], with  $\epsilon_r$  representing the increased dielectric constant. In the presence of valley degree of freedom, if we ignore the Coulomb exchange between excitons from different valleys (equivalent to setting the excitons' center-of-mass momentum to zero [39]), the meanfield first order exciton energy correction is:  $\Delta E_\sigma \propto E_B n_\sigma^X$  [22], where  $n_\sigma^X$  is the excitation density and  $\sigma = \pm$  is the pump beam polarization (or exciton valley) index. Under an incoherent cw pump, the values of  $n_\sigma^X$  and  $n_c$  are not directly measurable. Considering that in forming an exciton one need to choose independently an electron and a hole, and that  $n_e = n_h = n_c$ , we can assume  $n_\sigma^X \sim n_c^2$  so that  $\Delta E_\sigma \sim n_c^2$ . Mathematically, when  $n_c$  is small (in units of  $a_B^2$ ), the Maclaurin series of  $n_\sigma^X$  reads:  $n_\sigma^X \approx a_\sigma + b_\sigma n_c + c_\sigma n_c^2$  with  $a_\sigma, b_\sigma, c_\sigma$  the expansion coefficients. It can be rewritten in vertex form  $n_\sigma^X = a'_\sigma + b'_\sigma (n_c - c'_\sigma)^2$ . We redefine the shifted  $n_c - c'_\sigma$  as  $n_c$  [40] and treat  $b'_\sigma$  as a fitting parameter denoted as  $f_\sigma$ . Finally, the sum of two  $n_c$ -independent terms  $a'_\sigma$  and  $-1/\epsilon_r^2$  is denoted as  $s_\sigma$ , and we reach the screened exciton energy:

$$\Delta E_\sigma^X(n_c) = (s_\sigma + f_\sigma n_c^2) E_B. \quad (2)$$

Combining Eqs. (1) and (2), we can express the PL peak energy for excitons from different valleys as:

$$E_\sigma(n_c) = E_g + \Delta E_g(n_c) + (s_\sigma + f_\sigma n_c^2) E_B, \quad (3)$$

where  $s_\sigma$  and  $f_\sigma$  are fitting parameters corresponding to the spin imbalance of the pump. Fig. 2 shows the theoretical curves plotting along with experimental data,

from where we can estimate the free carrier density  $n_c \sim 10^9 - 10^{10} \text{ cm}^{-2}$  similar to that observed in a previous experiment [9]. Note that if we extend the theoretical plot of Eq. (3) beyond the current experimental range, the PL peak will exhibit blueshift behavior when the energy correction term  $f_\sigma n_c^2$  surpasses the other terms. In this case, the meanfield first order perturbation theory breaks down and a more rigorous calculation would be required. Nevertheless, based on the existing experimental data we can see that the nonlinear dependence of  $n_X$  on  $n_c$  could be responsible for the redshift-blueshift crossover, which was previously explained by the Lennard-Jones type potential in real space [9].

Our experimental results can be repeated in other MoS<sub>2</sub> samples using different fabrication techniques. In the supplemental materials, we show the existence of the spin splitting in a CVD grown MoS<sub>2</sub> monolayer without hBN capping and a mechanically exfoliated MoS<sub>2</sub> monolayer. Although the exciton energy in these samples vary piece by piece, however, the spin splitting does not change too much under the same pumping condition. This rules out the possibility that the spin splitting results from the interaction with the capping hBN layer or some defects in the growth process. In addition, the spin splitting also exists in a MoS<sub>2</sub> monolayer using a pure silicon and hBN substrate (shown in the supplemental materials), excluding the effect from the substrate.

With increasing the temperature, both the excitons A and B will shift to lower energies. In Fig3, we repeat the measurements at different temperatures (15K, 50K, 100K, 150K, 200K, 250K and 300K). At higher temperature, the circular polarization of the photoluminescence decreases due to the phonon assisted intervalley scattering, in agreement of [30, 41–43]. Although the spectra corresponding to the exciton B can keep the circular polarization even at room temperature (10%), the spin splitting under the circularly polarized pumping approaches zero at around 200K, as shown in Fig3 (b)(d).

*Conclusion.* We show experimentally and theoretically that spin dependent exciton exciton interaction under a spin-biased pump can lead to exciton energy splitting between different valleys in a MoS<sub>2</sub> ML. The spin splitting can be tuned at much lower power density (MW/cm<sup>2</sup>) approaching 18meV, which is much more effective compared with the optical Stark effect. In addition, it does not need external magnetic field or stacking different materials. The CW-pumping created spin splitting provides a reliable way to explore the valley degree of freedom for MoS<sub>2</sub> ML and it is readily applicable to the investigation of the spin dynamics of TMD exciton-polariton systems.

TG acknowledges supports from National Natural Science Foundation of China (NSFC, No. 11874278) and supports from Young scholar 1000 Talents plan. GL thanks Dr. Dmitry Efimkin for useful discussions.

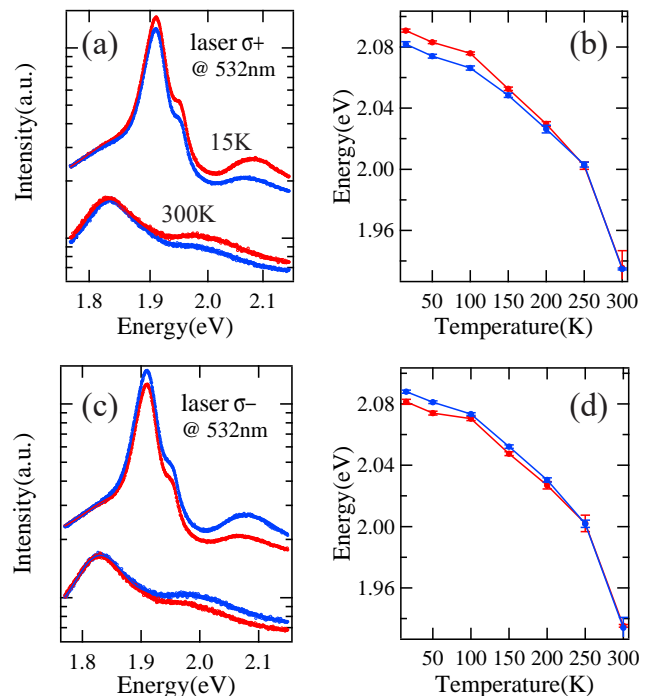


FIG. 3: PL spectra of the MoS<sub>2</sub> ML at different temperatures. (a)(c) Optical spectra at 15 K and 300 K pumping by a right- and left-handed circularly polarized laser respectively. Power density: 0.03MW/cm<sup>2</sup>. (b)(d) Exciton energy against temperature.

- 
- [1] X. Xu, W. Yao, D. Xiao, T. F. Heinz, Nat. Phys. **10**, 343 (2014).
  - [2] Q. H. Wang, K. Kalantar-Zadeh, A. Kis, J. N. Coleman, M. S. Strano, Nat. Nanotechnol. **7**, 699 (2012).
  - [3] G. Wang, A. Chernikov, M. M. Glazov, T. F. Heinz, X. Marie, T. Amand, and B. Urbaszek, Rev. Mod. Phys. **90**, 021001 (2018).
  - [4] A. Splendiani, L. Sun, Y. Zhang, T. Li, J. Kim, C.-Y. Chim, G. Galli, and F. Wang, Nano Lett. **10**, 1271 (2010).
  - [5] Kin Fai Mak, Changgu Lee, James Hone, Jie Shan, and Tony F. Heinz, Phys. Rev. Lett. **105**, 136805 (2010).
  - [6] T. Mueller and E. Malic, Npj 2D Mater. Appl. **2**, 29 (2018).
  - [7] A. Chernikov, C. Ruppert, H. M. Hill, A. F. Rigosi, and T. F. Heinz, Nat. Photon. **9**, 466 (2015).
  - [8] G. Aivazian, H. Yu, S. Wu, J. Yan, D. G. Mandrus, D. Cobden, W. Yao, and X. Xu, 2D Materials **4**, 025024 (2017).
  - [9] E. J. Sie, A. Steinhoff, C. Gies, C. H. Lui, Q. Ma, M. Rösner, G. Schönhoff, F. Jahnke, T. O. Wehling, Y.-H. Lee, J. Kong, P. Jarillo-Herrero and N. Gedik, Nano Lett. **17**, 4210 (2017).
  - [10] Di Xiao, Gui-Bin Liu, Wanxiang Feng, Xiaodong Xu, and Wang Yao, Phys. Rev. Lett. **108**, 196802 (2012).
  - [11] Gui-Bin Liu, Wen-Yu Shan, Yugui Yao, Wang Yao, and Di Xiao, Phys. Rev. B **88**, 085433 (2013).

- [12] J. R. Schaibley, H. Yu, G. Clark, P. Rivera, J. S. Ross, K. L. Seyler, W. Yao, and X. Xu, *Nat. Rev. Mater.* **1**, 16055 (2016).
- [13] Yilei Li, Jonathan Ludwig, Tony Low, Alexey Chernikov, Xu Cui, Ghidewon Arefe, Young Duck Kim, Arend M. van der Zande, Albert Rigosi, Heather M. Hill, Suk Hyun Kim, James Hone, Zhiqiang Li, Dmitry Smirnov, and Tony F. Heinz, *Phys. Rev. Lett.* **113**, 266804 (2014).
- [14] Ajit Srivastava, Meinrad Sidler, Adrien V. Allain, Dominik S. Lembke, Andras Kis and A. Imamolu, *Nat. Phys.* **11**, 141 (2015).
- [15] David MacNeill, Colin Heikes, Kin Fai Mak, Zachary Anderson, Andor Kormnyos, Viktor Zlyomi, Jiwoong Park, and Daniel C. Ralph, *Phys. Rev. Lett.* **114**, 037401 (2015).
- [16] G. Aivazian, Z. Gong, A. M. Jones, R.-L. Chu, J. Yan, D. G. Mandrus, C. Zhang, D. Cobden, W. Yao, and X. Xu, *Nat. Phys.* **11**, 148 (2015).
- [17] Chuan Zhao, Tenzin Norden, Peiyao Zhang, Puqin Zhao, Yingchun Cheng, Fan Sun, James P. Parry, Payam Taheri, Jieqiong Wang, Yihang Yang, Thomas Scrace, Kaifei Kang, Sen Yang, Guo-xing Miao, Renat Sabirianov, George Kioseoglou, Wei Huang, Athos Petrou and Hao Zeng, *Nat. Nanotechnol.* **12**, 757 (2017).
- [18] Tenzin Norden, Chuan Zhao, Peiyao Zhang, Renat Sabirianov, Athos Petrou and Hao Zeng, *Nat. Commun.* **10**, 4163 (2019).
- [19] Jing Zhang, LuoJun Du, Shun Feng, Run-Wu Zhang, Bingchen Cao, Chenji Zou, Yu Chen, Mengzhou Liao, Baile Zhang, Shengyuan A. Yang, Guangyu Zhang and Ting Yu, *Nat. Commun.* **10**, 4226 (2019).
- [20] Edbert J. Sie, James W. McIver, Yi-Hsien Lee, Liang Fu, Jing Kong, and Nuh Gedik, *Nat. Mater.* **14**, 290 (2015).
- [21] Jonghwan Kim, Xiaoping Hong, Chenhao Jin, Su-Fei Shi, Chih-Yuan S. Chang, Ming-Hui Chiu, Lain-Jong Li, Feng Wang, *Science* **346**, 1205 (2014).
- [22] J. Fernández Rossier, C. Tejedor, L. Muñoz, and L. Viña, *Phys. Rev. B* **54**, 11582 (1996).
- [23] H. Haug and S. Schmitt-Rink, *Prog. Quant. Electron* **3**, 1 (1985).
- [24] C. Ell, R. Blank, S. Benner, and H. Haug, *J. Opt. Soc. Am. B* **6**, 2006 (1989).
- [25] S. Wang, S. Li, T. Chervy, A. Shalabney, S. Azzini, E. Orgiu, J. A. Hutchison, C. Genet, P. Samor, and T. W. Ebbesen, *Nano Lett.* **16**, 4368 (2016).
- [26] X. Liu, T. Galfsky, Z. Sun, F. Xia, E. Lin, Y.-H. Lee, S. Kna-Cohen, and V. M. Menon, *Nat. Photon.* **9**, 30 (2015).
- [27] Kin Fai Mak, Keliang He, Jie Shan and Tony F. Heinz, *Nat. Nanotechnol.* **7**, 49 (2012).
- [28] Z. Y. Zhu, Y. C. Cheng, and U. Schwingenschlgl, *Phys. Rev. B* **84**, 153402 (2011).
- [29] S. Dal Conte, F. Bottegoni, E. A. A. Pogna, D. De Fazio, S. Ambrogio, I. Bargigia, C. D'Andrea, A. Lombardo, M. Bruna, F. Ciccacci, A. C. Ferrari, G. Cerullo, and M. Finazzi, *Phys. Rev. B* **92**, 235425 (2015).
- [30] G. Sallen, L. Bouet, X. Marie, G. Wang, C. R. Zhu, W. P. Han, Y. Lu, P. H. Tan, T. Amand, B. L. Liu and B. Urbaszek, *Phys. Rev. B* **86**, 081301(R) (2012).
- [31] Jason W. Christopher, Bennett B. Goldberg, and Anna K. Swan, *Sci. Rep.* **7**, 14062 (2017).
- [32] Theory parameters:  $E_g = 2.15$  eV and  $E_B = 0.44$  eV [3];  $\omega = 0$  (static screening);  $\epsilon_0 = \epsilon_r \epsilon_0$  with  $\epsilon_r = 4.47$  [44] and  $\epsilon_0$  the vacuum permittivity;  $m_e = 0.53 m_0$  and  $m_h = 0.65 m_0$  [45] with  $m_0$  the free electron mass; Fig.2(b):  $s_\sigma = 2.87 \times 10^{-2}$  and  $f_\sigma = 2.98 \times 10^{-6} \mu m^4$ ; Fig.2(d):  $s_+ = 3.15 \times 10^{-2}$ ,  $f_+ = 4.47 \times 10^{-6} \mu m^4$  and  $s_- = 1.81 \times 10^{-2}$ ,  $f_- = 5.70 \times 10^{-8} \mu m^4$ ; Fig.2(f)  $s_+ = 2.22 \times 10^{-2}$ ,  $f_+ = 6.54 \times 10^{-7} \mu m^4$  and  $s_- = 3.11 \times 10^{-2}$ ,  $f_- = 5.07 \times 10^{-6} \mu m^4$ .
- [33] Chongyun Jiang, Abdullah Rasmita, Weigao Xu, Atac Imamoglu, Qihua Xiong and Wei-bo Gao, *Phys. Rev. B* **98**, 241410(R) (2018).
- [34] L. Viña, L. Muñoz, E.Pérez J. Fernández Rossier, C. Tejedor and K. Ploog, *Phys. Rev. B* **54**, R8317(1996).
- [35] Zheng Sun, Z. Y. Xu, Yang Ji, B. Q. Sun, B. R. Wang, S. S. Huang, and H. Q. Ni, *Appl. Phys. Lett.* **90**, 071907 (2007).
- [36] T C. Damen, Luis Viña, J. E. Cunningham, Jagdeep Shah and L. J. Sham, *Phys. Rev. Lett.* **67**, 3432 (1991).
- [37] P. Le Jeune, X. Marie, T. Amand, F. Romstad, F. Perez, J. Barrau and M. Brousseau, *Phys. Rev. B* **58**, 4853 (1998).
- [38] Combescot, Shiue-Yuan Shiau, *Excitons and Cooper Pairs: Two Composite Bosons in Many-Body Physics* (Oxford University Press, Oxford, UK, 2016).
- [39] H. Yu, G. Bin Liu, P. Gong, X. Xu, and W. Yao, *Nat. Commun.* **5**, 3876 (2014).
- [40] If  $n_\sigma^X$  is expanded only up to a linear term in  $n_c$ ; or in the quadratic expansion the linear term is kept, then in both cases the fitted coefficient of the highest order term would be negative for some data. Physically it means that the exciton density decreases with the increase of free carrier density, which is unreasonable. Therefore, the fitting expression of Eq. (2) is quadratic without a linear term.
- [41] Hualing Zeng, Junfeng Dai, Wang Yao, Di Xiao and Xiaodong Cui, *Nat. Nanotechnol.* **7**, 490(2012)
- [42] D. Lagarde, L. Bouet, X. Marie, C. R. Zhu, B. L. Liu, T. Amand, P. H. Tan, and B. Urbaszek, *Phys. Rev. Lett.* **112**, 047401(2014)
- [43] Sanfeng Wu, Chunming Huang, Grant Aivazian, Jason S. Ross, David H. Cobden, and Xiaodong Xu, *ACS Nano* **7**, 2768 (2013).
- [44] G. Wang, I. C. Gerber, L. Bouet, D. Lagarde, A. Blochchi, M. Vidal, E. Palleau, T. Amand, X. Marie, and B. Urbaszek, *2D Mater.* **2**, 045005 (2015).
- [45] Z. Jin, X. Li, J. T. Mullen, and K. W. Kim, *Phys. Rev. B* **90**, 045422 (2014).